UC San Diego
Oceanography Program Publications

Title
Observations of turbulence in the surf zone

Permalink
https://escholarship.org/uc/item/96h110j3

Journal
Journal of Geophysical Research, 99(C1)

Authors
George, R
Flick, R E
Guza, R T

Publication Date
1994-01-15

Data Availability
The data associated with this publication are available upon request.

Peer reviewed

eScholarship.org Powered by the California Digital Library
University of California

JOURNAL OF GEOPHYSICAL RESEARCH, VOL. 99, NO. C1, PAGES 801–810, JANUARY 15, 1994

Observations of turbulence in the surf zone

Ron George
Center for Coastal Studies, Scripps Institution of Oceanography, La Jolla, California

R. E. Flick
California Department of Boating and Waterways, La Jolla, California

R. T. Guza
Center for Coastal Studies, Scripps Institution of Oceanography, La Jolla, California

Turbulence generated by waves breaking on a natural beach is examined using hotfilm anemometer data. Turbulence intensity is estimated from dissipation rates determined from wavenumber spectra of short (1/8 s) hotfilm time series. The resulting Froude-scaled turbulence intensities are relatively uniform between the seabed and the wave trough level and are similar in vertical structure but lower in magnitude than in existing laboratory studies. The magnitudes of the turbulence intensities observed in both the field and laboratory are consistent with an existing macroscopic model of bore dissipation in the surf zone. Scaling by this bore model relates turbulence intensities generated by monochromatic waves in small-scale laboratory experiments to those generated by random waves in the natural surf zone.

1. Introduction

Shoreward propagating sea and swell energy is transformed in the surf zone into motions of many different types and scales, including steady currents, low-frequency waves, organized vortical flows, and high-Reynolds-number turbulence [*Battjes*, 1988]. Much attention has been devoted to the relatively energetic sea-swell and infragravity frequency bands (nominally 0.005 Hz to 0.5 Hz). Less is known about higher frequency turbulent motions, which contain only a small fraction of the total kinetic energy of the nearshore velocity field, but usually dissipate most of the shoreward energy flux. Although many laboratory studies of surf zone turbulence have been conducted using breaking progressive waves [e.g., *Stive*, 1980, *Nadaoka and Kondoh*, 1982, and *Hattori and Aono*, 1985], hydraulic jumps [*Resch and Leutheusser*, 1972], and solitons [*Skjelbreia*, 1987], experiments in the natural surf zone have been hindered by instrumentation difficulties.

New measurements of turbulence intensity in the natural surf zone are described in section 2. In section 3, the wavenumber spectrum, $\Phi(\kappa)$, is obtained from a point measurement in this strongly oscillatory flow using Taylor's hypothesis (subject to a condition similar to *Lin's* [1953] criterion for the application of Taylor's hypothesis in shear flow). From the inertial subrange of $\Phi(\kappa)$, we estimate the dissipation rate (ε) and then the rms turbulence intensity (u') using a form of the classical relationship $\varepsilon = u'^3/l$ where l, the scale of the most energetic turbulent eddies, is a fraction of the water depth (h). In section 4 we show that Froude-scaled surf zone turbulence levels, $u'/(gh)^{1/2}$, are smaller in the natural surf zone than in existing laboratory studies. However, the turbulence levels in both the field and the laboratory are consistent with an existing bore model which accounts for differences in wave frequencies, wave-height to water-depth ratios, breaking intensities, and percentages of broken waves.

Copyright 1994 by the American Geophysical Union.

Paper number 93JC02717.
0148-0227/94/93JC-02717$05.00

2. Experiments

Experiments were conducted at Scripps Beach, La Jolla, California, during six days in March and April 1992 in water depths between 28 and 274 cm. This is a fine-grained gently sloping (about 1 in 40) sandy beach with relatively small alongshore depth changes. Waves broke by both spilling and plunging. Significant waveheights (H_0) in 7-m water depth (a few hundred meters offshore) ranged from 50 to 120 cm.

Data were collected from three vertically separated hotfilm anemometers, two electromagnetic (EM) current meters with 4-cm spherical probes, one pressure sensor, and a videocamera recorder (VCR). The hotfilms were Thermo-Systems, Inc. (TSI) model 1755 constant-temperature anemometers with 1210-60 W cylindrical quartz-coated platinum probes. Although the most rugged of the cylindrical TSI probes, they are fragile and many probes were broken. The more rugged conical 1230 W probes have less desirable symmetry and gain characteristics. Relatively low operating temperatures (40°C, producing an overheat ratio of roughly 8%) were used to avoid bubble formation on the probe.

All instruments except the VCR were mounted on a steel pipe frame (Figure 1) which was lowered daily by crane from Scripps pier and anchored to the seabed 10 m up-drift (in the alongshore direction) from the pier. The hotfilms were located 40 cm up-drift from the EM current meters, and the pressure sensor was buried about 10 cm in the seabed. The VCR was used to determine the frequency and intensity of wave breaking. However, the time synchronization between the videocamera and the hotfilms was inadequate to determine which individual waves in the hotfilm time series were broken. Anti-aliasing analog filters were applied to the hotfilm and current meter signals before digitization.

There were 70 data runs, each of 512-s duration. From the

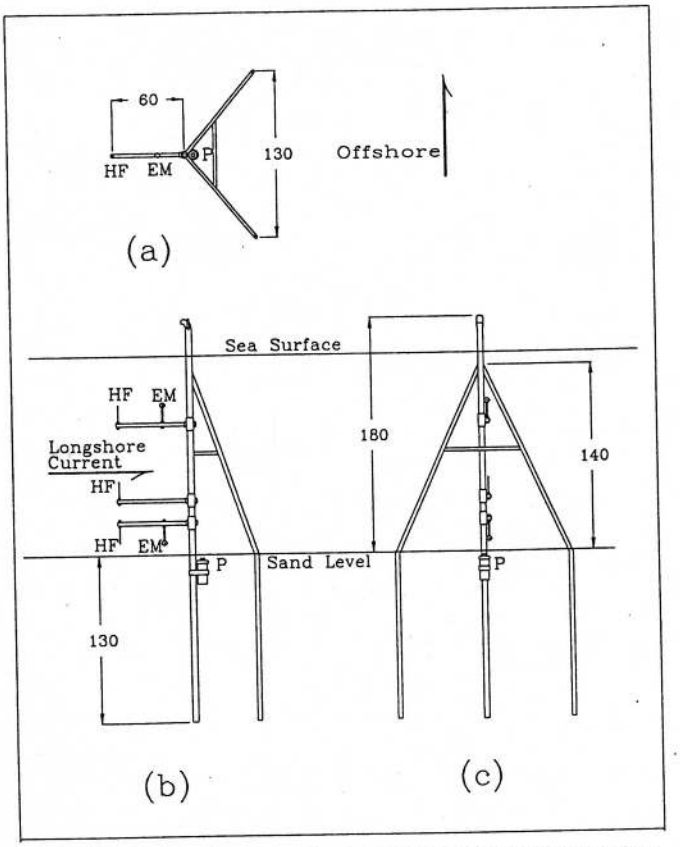

Fig. 1. Instrument package mounting frame with positions of hotfilms (HF), electromagnetic current meters (EM), and pressure sensor (P). Dimensions are in centimeters. (*a*) Plan view. (*b*) View looking cross-shore. (*c*) View looking alongshore.

resulting potential 210 hotfilm time series, those with broken probes, instruments out of the water, or questionable calibrations were rejected, leaving 125 usable hotfilm time series. The vertical positions of the hotfilms are shown in Figure 2. While the broad wave height distribution produces no consistent "break point," breaking waves were infrequent deeper than $h/H_0 = 3.0$.

Estimates of the aeration in the air bubble region (foam) on the leading face of a bore range from a few percent to as much as 40 percent [*Fuhrboter*, 1970]. Spurious signals from the constant-temperature hotfilm anemometer caused by the bubbles (because air has much lower heat capacity than water) were removed from the raw hotfilm signal as described in Appendix A.

Because stable calibrations between the calibration facility and the ocean could not be maintained, the hotfilms were calibrated in situ using EM current meters located at the same vertical elevation as the upper and lower hotfilm probes (see Appendix B). The mean of the EM current meter signals was used to calibrate the nearly equidistant middle hotfilm. Figure 3 shows time series of sea surface elevation and hotfilm speeds for cases in which most (Figures 3*a*-3*d*) and few (Figures 3*e*-3*g*) waves were broken. The increase in high-frequency velocity fluctuations with increased wave breaking (compare Figures 3*g* and 3*c*) is much larger than the corresponding increase in wave height (Figures 3*a* and 3*e*) and orbital speeds (Figures 3*b* and 3*f*), suggesting that breaking waves (not vortex shedding or vibration of the instruments) generate the high-frequency fluctuations.

3. RESULTS

Methods of Estimating Turbulence Intensity

Turbulence in steady free-stream flow or towed-body experiments is often defined as the fluctuation about the mean velocity [e.g., *Hinze*, 1975]. In a laboratory surf zone with monochromatic plane waves, turbulence has been defined analogously as the deviation from an ensemble average of velocities at the same wave phase [*Flick et al.*, 1981]. The stochastic nature of natural orbital wave velocities precludes use of this definition here.

Thornton [1979] separated surf zone orbital wave energy from turbulence by defining the wave orbital motions as the velocity fluctuations coherent with the sea surface elevation and assuming that all incoherent velocities are turbulence. However, this definition does not include as turbulence the largest scale eddies which do influence the sea surface [*Nadaoka et al.*, 1989] and may contribute significantly to the Reynolds' stresses. Other disadvantages are that nonlinearity [e.g., *Flick et al.*, 1981], and (for horizontal velocities) directional spreading [*Kitaigorodskii et al.*, 1983] in a nonturbulent wave field reduce the coherence between sea surface elevation and velocity. While the relative underestimation of the more energetic orbital flow is small [*Thornton*, 1979], overestimation of the relatively low turbulent energy levels may be large.

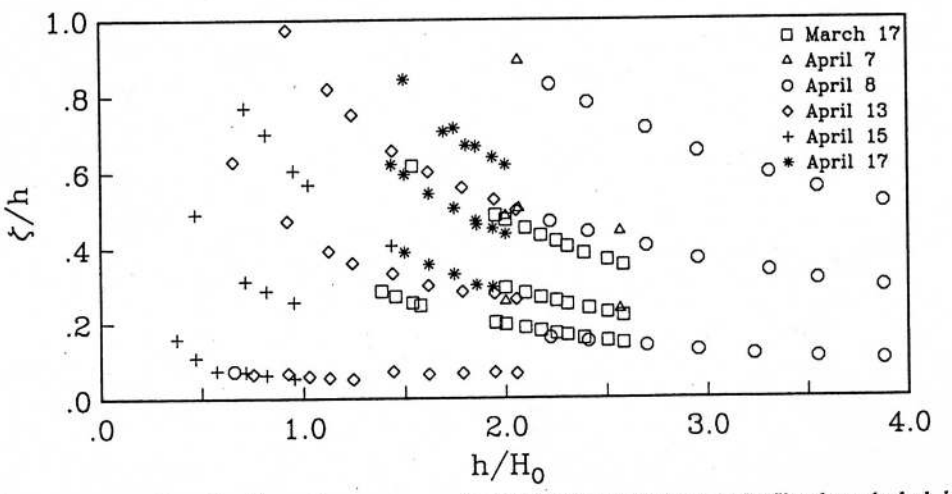

Fig. 2. Relative vertical position of hotfilm probes versus normalized depth; ζ is elevation of the hotfilm above the bed, h is water depth, and H_0 is the significant wave height in 7-m depth.

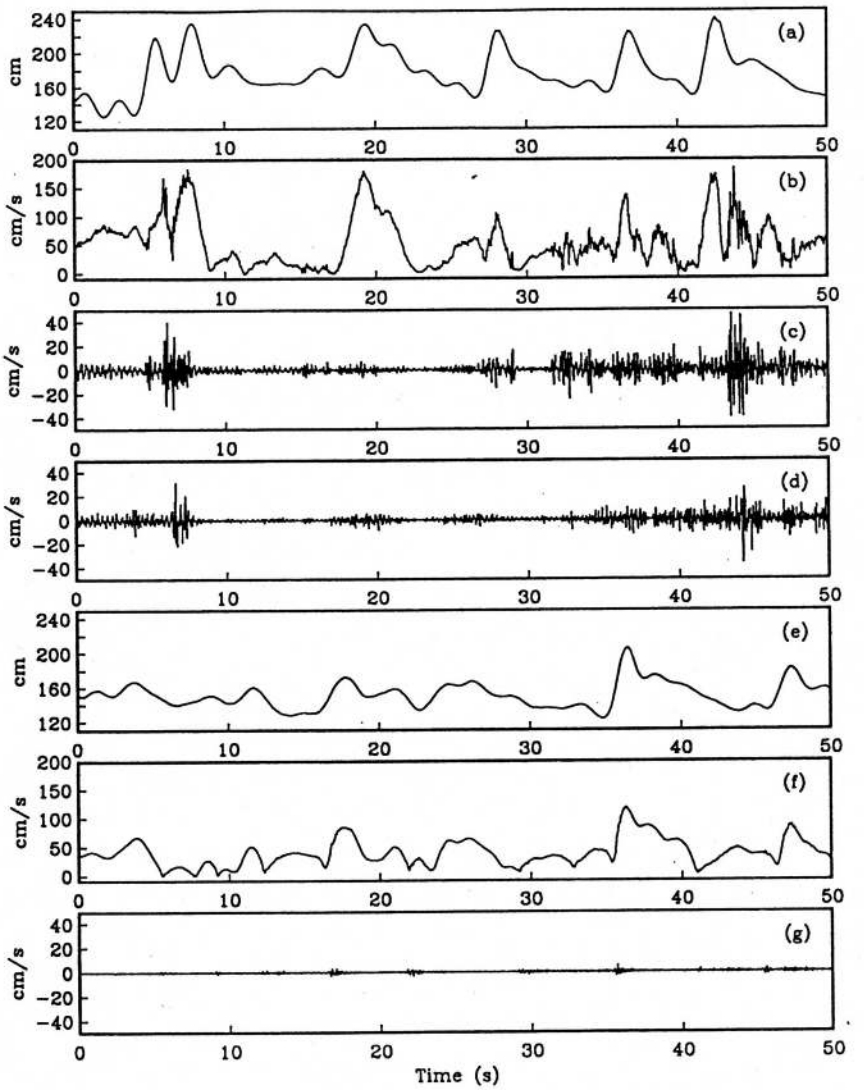

Fig. 3. Representative time series *a-d* in surf zone; 60% of waves broken; h=178 cm; $\gamma=H/h$=0.33. (*a*) Sea surface elevation from the pressure data and linear theory. (*b*) Hotfilm speed. (*c* and *d*) Hotfilm high-pass filtered at f_e=2.35 Hz. Elevation above bed is (*c*) ζ =119 cm and (*d*) ζ=84 cm. (*e-g*) Seaward of surf zone; 3% of waves broken; h=149 cm; $\gamma=H/h$=0.28; ζ=119 cm. (*e*) Sea surface elevation. (*f*) Hotfilm speed. (*g*) Hotfilm high-pass filtered at f_e.

The hotfilm frequency spectra (Figure 4) typically exhibit turbulent (inertial subrange slope is $f^{-5/3}$) and orbital wave (f^{-3} [*Thornton*, 1979]) regimes. However, the transition (where the slope changes) between the two regimes indicates only where dominance changes, not the low-frequency end of the turbulent inertial subrange. The overlap region prevents accurate estimation of turbulence intensity by high-pass filtering above a single "cutoff frequency" [*Nadaoka and Kondoh*, 1982]. Because the coherence and cutoff methods are potentially inaccurate, we calculate the turbulence intensity from the dissipation rate as described below.

Taylor's Hypothesis

The dissipation rate, ε, of a one-dimensional wavenumber spectrum $\Phi(\kappa)$ may be found from the universal form of the inertial subrange

$$\Phi(\kappa) = \alpha\varepsilon^{2/3}\kappa^{-5/3} \tag{1}$$

[*Tennekes and Lumley*, 1972], where κ is the wavenumber magnitude and α (nominally 0.5) is the one-dimensional Kolmogorov constant. We first estimate $\Phi(\kappa)$ from the measured frequency spectrum $\Phi(f)$.

Laboratory experiments commonly concern relatively weak turbulence intensity (u') in a spatially and temporally steady advective flow (U):

$$U >> u'. \tag{2}$$

In this case, Taylor's hypothesis can be used to convert the entire frequency spectrum (from time series measured at a fixed point) to the desired wavenumber spectrum:

$$\Phi(\kappa) = \frac{\Phi(f)}{2\pi / U} \tag{3}$$

where

$$\kappa = \frac{2\pi f}{U}. \tag{4}$$

In the surf zone, U denotes all nonturbulent flow, including orbital wave, lower frequency, and mean. In addition to satisfying (2), U must also be steady over the record length to apply (3) because changes in U will distort the f-κ transformation (4). *Lin* [1953] considered a similar type of distortion in strong

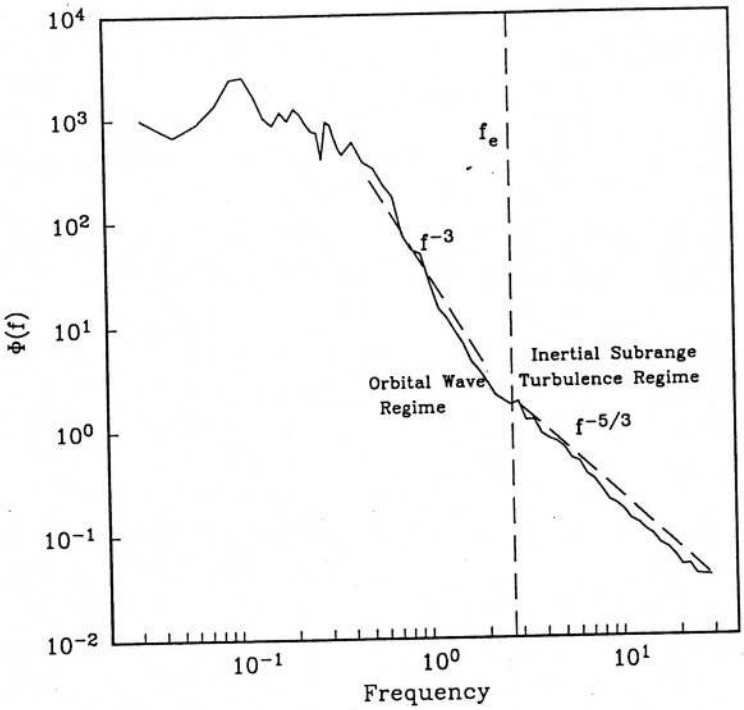

Fig. 4. Frequency spectrum of a typical 512-s hotfilm time series, showing orbital wave (f^{-3} slope) and inertial subrange turbulent ($f^{-5/3}$ slope) regimes: h=134 cm; ζ/h=0.29; Degrees of freedom increase with frequency from 62 to11,000.

shear flows and suggested that Taylor's hypothesis may be applied to the high wavenumber turbulent flow fluctuations only if the nonuniformity of the advection velocity over the eddy size is small compared to the advection velocity itself:

$$\kappa >> \frac{2\pi\, dU/dz}{U}, \tag{5}$$

where z is the vertical (transverse) axis. The temporal unsteadiness in the present case is analogous to the spatial shear. We modify Lin's criterion (5) for use in temporally unsteady flow to simply

$$U >> \Delta U, \tag{6}$$

where ΔU is the magnitude of the change in U.

One further criterion, unrelated to Taylor's hypothesis, insures that only the u component of the turbulent velocity is used in the dissipation rate estimate. This criterion [*Bradshaw*, 1971],

$$U >> V, W \tag{7}$$

where U, V, and W denote advective flow components in the cross-shore, longshore, and vertical directions, respectively, is necessary because the hotfilm probe senses flow from all directions. W was not measured, but we expect that $U >> W$ for the long advecting waves.

Because the orbital wave velocities that dominate the nearshore spectrum change over a wave period, and U must be steady over a record length, we screened short (1/8 s) sections of the 512-s time series for those satisfying (2), (6), and (7). To do this, each 512-s time series was first band-pass filtered into high- and low-frequency parts (u' and U, respectively) by filtering at f_e, approximately the transition between the orbital-wave and turbulent inertial regimes, where $f_e = \hat{U}/l \approx (g/h)^{1/2}$, ($l \approx h$ is the energetic eddy scale [*Battjes*, 1975] and $\hat{U} = (gh)^{1/2}$ is a common surf zone scaling velocity). Generally, f_e fell near the slope break in the velocity spectrum (e.g., Figure 4). U, V, ΔU, and u' were then estimated for each 1/8-s data segment. U was equal to the mean of each low-frequency, 1/8-s record, ΔU was the variability about that mean, and u' was the rms velocity of the corresponding high-frequency record. We emphasize that these very crude values of u' were used only for screening (i.e., verifying that (2) is satisfied). When a 1/8-s data segment did not satisfy all criteria (equations (2), (6), and (7)), the 1/8-s data "window" was moved in increments of 1/32 s through the data until the next usable section was found. The >> factor for all criteria was chosen as 5. Varying the factor from 4 to 7 typically produced 10% variation in the resulting dissipation-rate-based u' estimate. Data not meeting all criteria were discarded. Selective rejection of data with similar wave phases (e.g., (2) is consistently violated near velocity zero-crossings) may bias the results to an unknown extent. However, about 45% of the data passed all criteria (with extremes of 5% and 65% for individual 512-s records) so the estimates below are based on a significant portion of the total data set.

Dissipation Rate

Each selected high-frequency 1/8-s data segment (containing eight samples, see Appendix A) was linearly detrended, the frequency spectrum calculated, and the wavenumber spectrum found from (3) and (4). The dissipation rate was calculated by applying (1) to the best fit $\kappa^{-5/3}$ line through the wavenumber spectrum. There was a wide range of spectral slopes. The mean for all 1/8-s pieces was -1.25, less than the expected -5/3, possibly owing to the effect of bubbles on the dissipation rate [*Wang*, 1985].

The individual dissipation rates from 1/8-s pieces within each 512-s record were highly variable, consistent with the large variability in the high-frequency time series of velocity (e.g., Figures 3*c*, 3*d*). Variability in 1/8-s ε estimates is also expected, owing to the relatively few points in the wavenumber spectrum

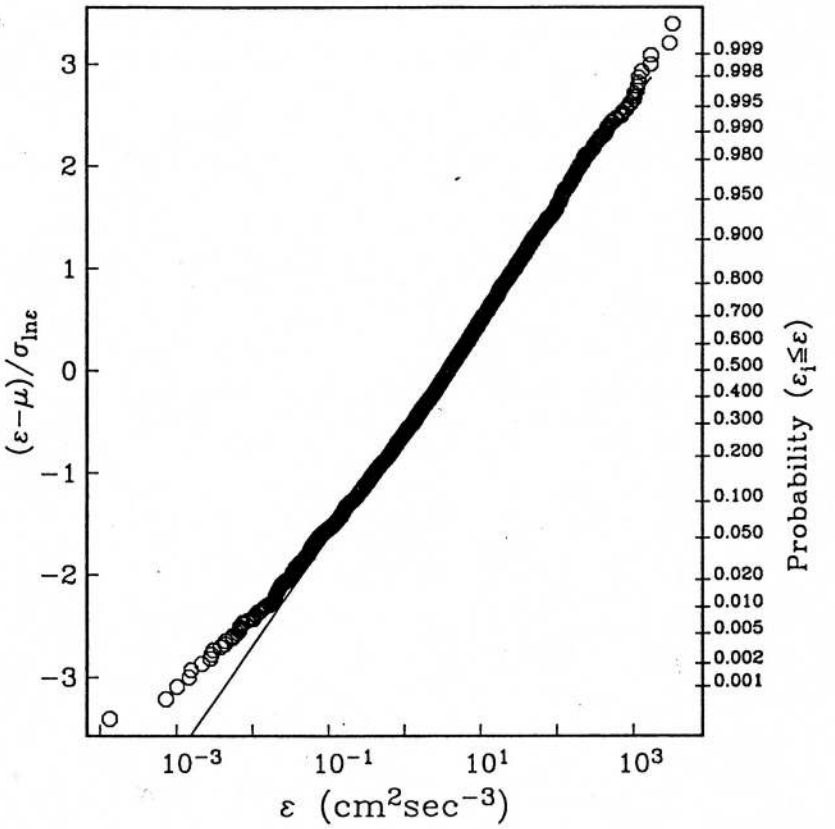

Fig. 5. Dissipation rates (based on 1/8-s subsections of a 512-s record) plotted on semilog paper versus probability ($\varepsilon_i \leq \varepsilon$). The right ordinate is stretched so that data from a lognormal distribution lie on a straight line. The corresponding "standardized normal random variable" $(\varepsilon-\mu)/\sigma_{\ln \varepsilon}$ is shown on the left ordinate. A straight line (ideal lognormal distribution) is fit through the data. The inverse slope of the line is $\sigma_{\ln \varepsilon}$ (here 1.95) and the zero-crossing is used to estimate μ (here 0.772).

inertial subrange available to determine the best $\kappa^{-5/3}$ line. Further work is needed to quantitatively assess the effects of statistical uncertainty of $\kappa^{-5/3}$ fits on the dissipation estimates.

A bulk dissipation rate for each 512-s record was then estimated as follows. *Oboukhov* [1962] suggested that intermittency in otherwise homogeneous turbulence produces an approximately lognormal distribution of dissipation rate. The dissipation rate in the natural surf zone appears highly intermittent (e.g., Figure 3*c*). If ε is a lognormally distributed random variable, e.g., $Z=\ln \varepsilon$ is normally distributed, then the expected value is

$$<\varepsilon>=\exp(\mu+\frac{\sigma^2_{\ln \varepsilon}}{2}) \tag{8}$$

where μ and $\sigma^2_{\ln \varepsilon}$, are the mean and variance of Z. The surf zone dissipation rates we observed are approximately lognormally distributed and the sample sizes small, so a graphical procedure [*Baker and Gibson*, 1987], (see our Figure 5) was used to estimate μ and $\sigma^2_{\ln \varepsilon}$ and thus $<\varepsilon>$ for each 512-s data segment. Uncertainty in the resulting $<\varepsilon>$ introduced by the estimation process [*Baker and Gibson*, 1987] produces uncertainty in the turbulence intensities ranging from ±3% to ±15%, with a mean of ±5%. Record lengths of 1/16- and 1/4-s produced turbulence intensities within ±10% of the 1/8-s values.

Kolmogorov [1962] defined $\sigma^2_{\ln \varepsilon}$ as the intermittency. Natural surf zone intermittencies ranged from about 2 to 12, with most values falling between 3 and 8, while deep-ocean values ranged from 3 to 7 [*Baker and Gibson*, 1987]. The highest intermittencies occurred where very few waves were broken.

In the natural surf zone, $<\varepsilon>$ (for a 512-s record) ranged from 5×10^{-1} to 5×10^{2} cm²/s³, compared to 10^{-3} to 10^{-2} cm²/s³ in the equatorial undercurrent [*Crawford and Osborne*, 1980] and 10^{-2} to 10^{0} cm²/s³ in a tidal channel [*Grant et al.*, 1962].

Figure 6 shows all 125 $<\varepsilon>$ values separated into three categories which correspond roughly to the fraction of waves which were broken. The dissipation rates were smallest when $h/H_0 > 3.0$, where less than 5% of the waves were broken. As h/H_0 decreases, the fraction of broken waves generally increases and the normalized dissipation rate tends to increase.

Dissipation rates were also calculated using (1) applied to wavenumber spectra produced by applying Taylor's hypothesis to the frequency spectra of 512-s runs with U equal to the rms orbital velocity [*Lumley and Terray*, 1983]. This is a crude approximation because the criteria for Taylor's hypothesis (2), (6), and (7) are sometimes grossly violated. Dissipation rates were also calculated by integrating the dissipation spectrum, formed from the 512-s wavenumber spectrum, over the approximate inertial and viscous subranges [*Hinze*, 1975]. Both methods provided dissipation rates within roughly a factor of two of the $<\varepsilon>$ values calculated from wavenumber spectra of the 1/8-s records.

Turbulence Intensity

Turbulence intensity, u', was estimated from the dissipation rate, $<\varepsilon>$, using

$$u' = (\int_{\kappa_0}^{\infty} \Phi(\kappa)\delta\kappa)^{1/2}. \tag{9}$$

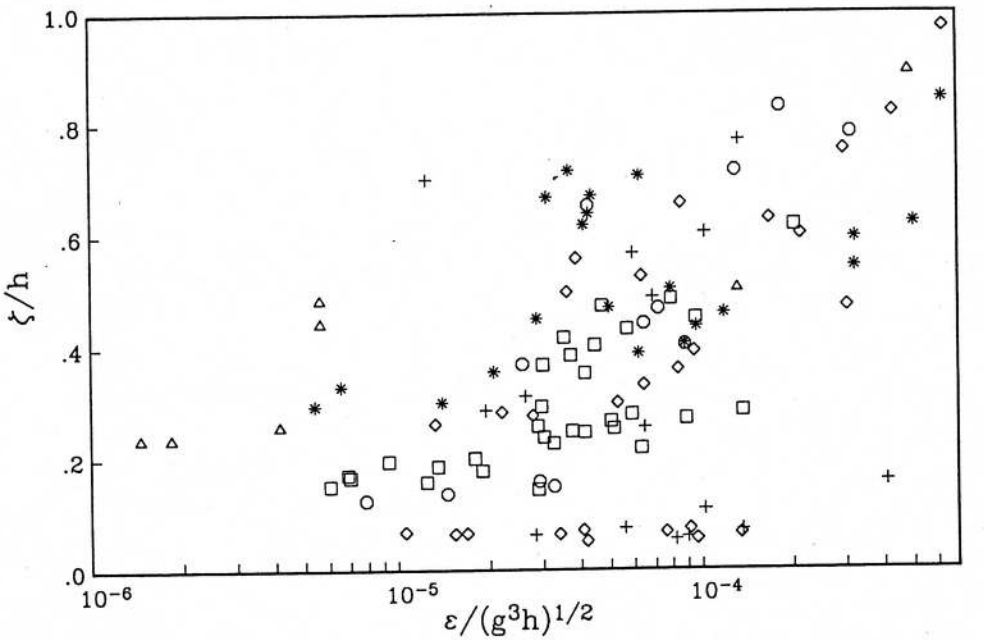

Fig. 6. Dissipation rates versus relative water column position. Normalization is by u^3/l, using $(gh)^{1/2}$ for u and h for l; h is the local mean depth.

We assume that the turbulent inertial subrange is of the universal form, defining $\Phi(\kappa)$ by (1), giving

$$u' = (\frac{3}{2}\alpha)^{1/2}(\frac{\varepsilon}{\kappa_0})^{1/3}. \quad (10)$$

Svendsen [1987] refined *Battjes* [1975] surf zone turbulence length scale estimate to $0.2h < l=2\pi/\kappa_0 < 0.3h$. We used $l = 0.25h$ (note the weak sensitivity of u' to the exact value of l), except for sensors closer to the bed than $0.25h$ that were influenced by the bottom boundary layer (i.e., $<\varepsilon>$ at the bottom sensor was larger than $<\varepsilon>$ at the middle sensor). In that case l was set equal to the distance to the bed.

For three-dimensional turbulence, the inertial dissipation method we have used (10) is consistent with *Gibson's* [1991] definition of turbulence: the inertial vortical forces are larger than the damping forces. This seems plausible in the (well-mixed) surf zone, because damping due to buoyancy is likely to be small. However, the method used does not include as turbulence the large two-dimensional eddies and "eddy-like flow" [*Nadaoka et al.*, 1989] because they are not dissipative.

Figure 7*a* shows that the turbulence intensities within the surf zone ($h/H_0 < 3.0$) are roughly 5-10% of the orbital wave velocities (i.e., the turbulent kinetic energy is less than 1% of the

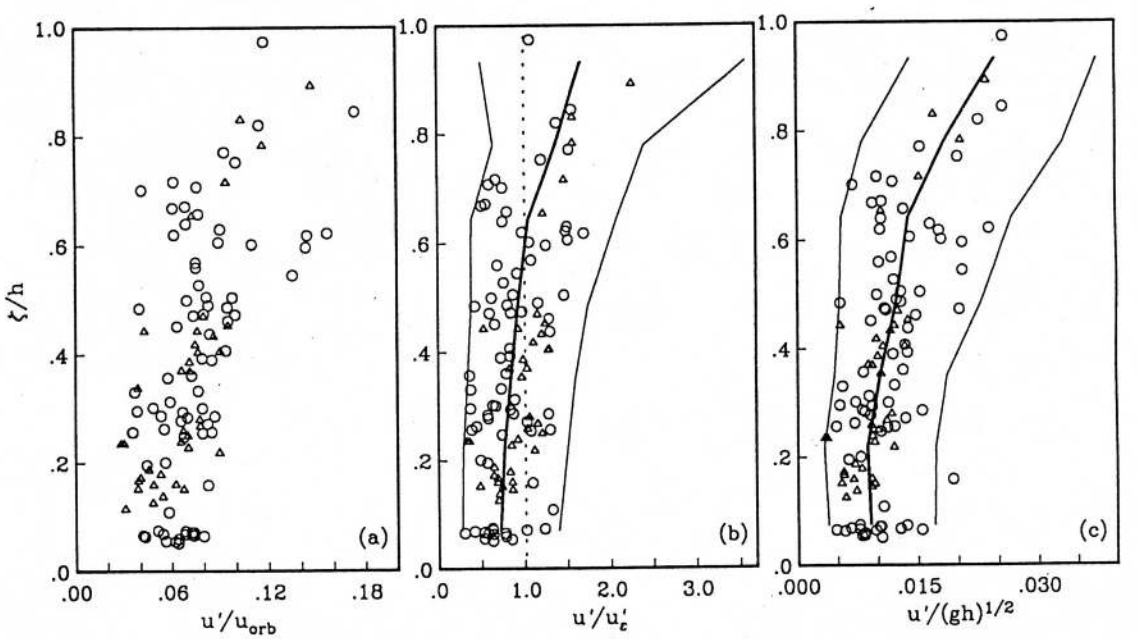

Fig. 7. Vertical profiles of turbulence intensity, u', for the 114 data points where $h/H_0 < 3.0$; u' is normalized by (*a*) u_{orb}, the rms orbital wave velocity; (*b*) equation (12), the bore dissipation model; and (*c*) $(gh)^{1/2}$, for comparison with laboratory data. In Figures 7*b* and 7*c* the bold line connects mean u' values in seven vertical bins, while the lighter lines indicate ±1 standard deviation plus the uncertainty introduced at the data processing steps mentioned in the text.

orbital wave energy). Turbulence intensities are largest near the surface and slowly decrease over the water column, consistent with strong mixing of turbulence from the surface downward.

Turbulence intensities were also estimated from the coherence between sea-surface elevation and cross-shore orbital velocity. They were generally greater than 30% of orbital wave velocities and independent of the fraction of broken waves. The directional spread (and perhaps nonlinearity) of the sea-swell wave field apparently reduce the coherence and severely bias this estimate of u'.

Turbulence intensities were compared to a model, based on the energy balance in a hydraulic jump, which for a train of periodic bores yields a depth-averaged dissipation rate [*Thornton and Guza*, 1983],

$$<\varepsilon>=\frac{1}{4}\rho g\gamma^3 hfB^3 \tag{11}$$

where f is the wave frequency, γ is the ratio of significant wave height to water depth, and B is a breaker coefficient related to the intensity of wave breaking. Following *Battjes* [1975], we assume that wave energy dissipation, turbulent kinetic energy production, and TKE dissipation are equal. Combining (10) and (11), using $\kappa_0 = 2\pi/(0.25h)$, and following *Thornton and Guza* [1983] in applying (11) to a random wave field, the bore dissipation model estimate of u' is

$$u'_\varepsilon = \gamma B(\frac{3}{8}\alpha)^{1/2}(\frac{fw_b}{4\pi}\rho g h^2)^{1/3}, \tag{12}$$

where w_b is the fraction of broken waves. B and w_b were determined from the videocamera records for each 512-s data run. Past estimates of B, found by fitting the observed wave height decay across both lab and field surf zones to model predictions based on (11), are about 1.0 [*Thornton and Guza*, 1983]. However, the precise relationship of B to breaking wave properties is unknown. We estimated B as the fraction of the bore face that was foam covered; the range was roughly 0.4 to 0.9 with a mean value for all data of 0.7. The broken-wave fractions varied from less than 0.1 to near 1.0 and the wave-height to water-depth ratio, γ, varied from 0.2 to 0.6.

The ratio u'/u'_ε is surprisingly near 1.0 (Figure 7*b*), considering that both u' and u'_ε are rather roughly estimated. The vertically averaged deviation of u'/u'_ε from 1.0 is about +0.05. Turbulence intensities were also Froude scaled (i.e., normalized by $(gh)^{1/2}$ [*Svendsen*, 1987]) in Figure 7*c* for comparison with laboratory data in the following section.

4. COMPARISON TO LABORATORY RESULTS

The present results are compared to previous laboratory results from *Stive* [1980] and *Hattori and Aono* [1985] (hereinafter H&A) in Figure 8, where u' is Froude scaled. While the weak dependence on vertical position is similar in the field and laboratory profiles, the scaled mean field turbulence intensity is only 1/4 to 1/2 of the laboratory values.

These laboratory studies used monochromatic and unidirectional waves, each of which breaks with about the same intensity. However, naturally occurring waves are stochastic with a mix of unbroken and broken waves of various heights and frequencies. These complexities are heuristically included in the bore-model-based estimates of turbulence intensity ((12) and Figure 7*b*). The bore model can also be applied to monochromatic waves by setting both the breaker coefficient and broken-wave fraction equal to 1.0 and using observed values of γ. This scaling (Figure 9) improves the agreement (relative to Froude scaling) of the lab and field u' values. The mean deviation of u'/u'_ε from unity is about +0.35 for Stive and -0.20 for H&A, compared to +0.05 for the field data.

Stive separated turbulent and wave motions by ensemble phase averaging, which probably slightly overestimates the turbulence intensity because of irregularities (unrelated to turbulence) in paddle-generated waves [*Svendsen*, 1987]. This is consistent with $u'/u'_\varepsilon > 1$ as observed for the Stive data (Figure 9*a*).

The bore-model estimates of u'_ε for H&A may be biased low because their data were taken over a flat bed shoreward of a 1/20 beach slope which extended from deep water to near the break point. In their experiment, γ decreased from roughly 0.8 near the

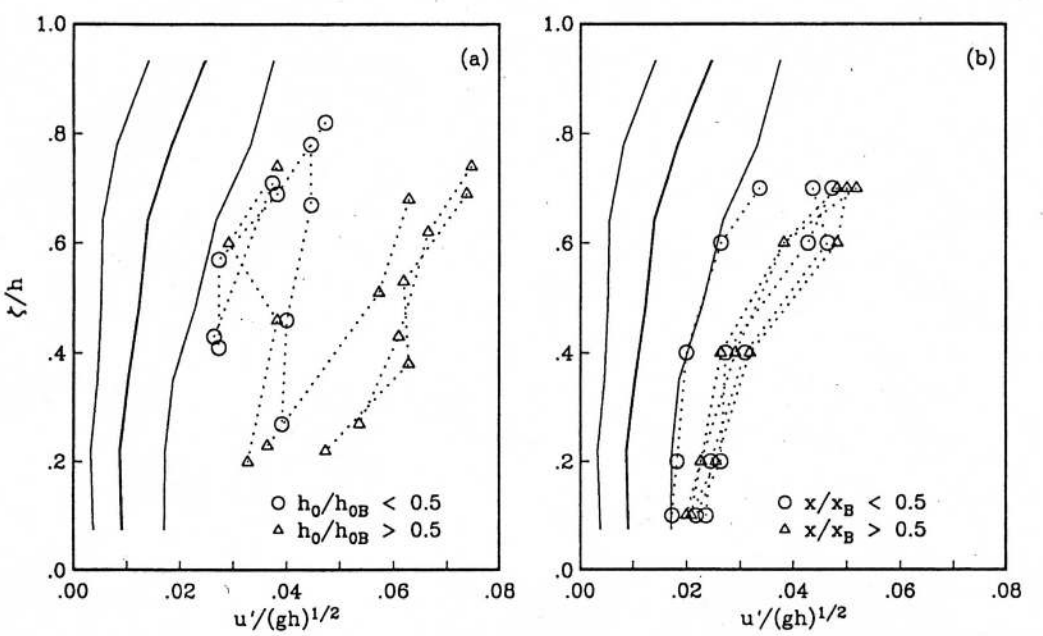

Fig. 8. Vertical profiles of turbulence intensity, u', scaled by $(gh)^{1/2}$). Field mean and bounds (solid lines) are from Figure 7*c*. Laboratory results are from (*a*) *Stive* [1980] and (*b*) *Hattori and Aono* [1985]. The laboratory data are sorted by (*a*) h_0/h_{0B}, the ratio of local depth to breaking depth; and (*b*) x/x_B, the ratio of distance from shore to surf zone width.

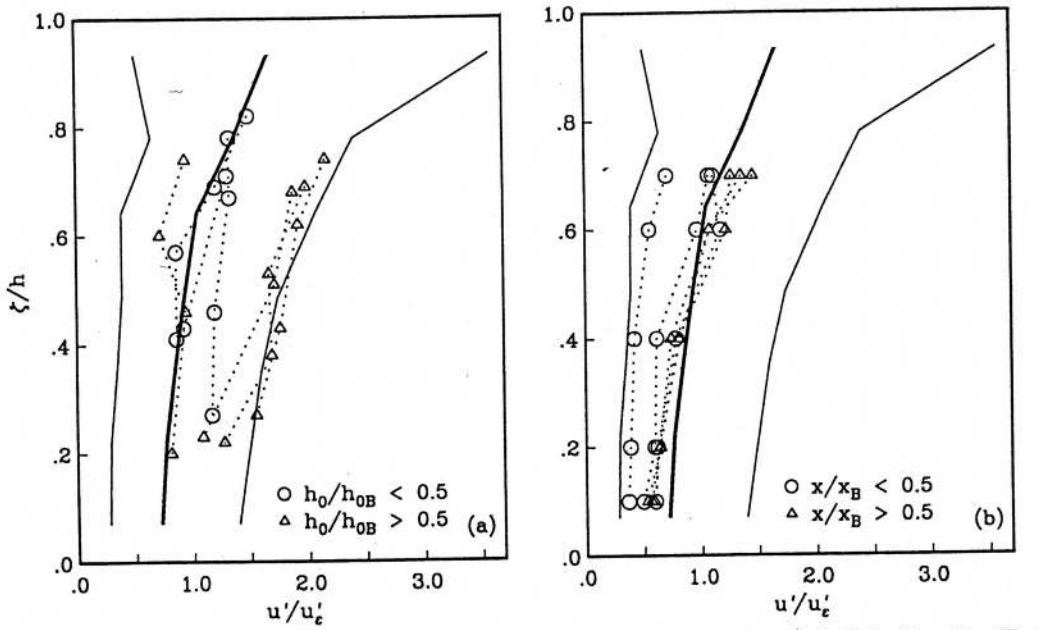

Fig. 9. Vertical profiles of turbulence intensity, u', scaled by u'/u'_ε (12). Field mean and bounds (solid lines) are from Figure 7*b*. Laboratory data are from (*a*) *Stive* [1980] and (*b*) *Hattori and Aono* [1985].

break point to 0.4 as the bores progressed shoreward (this variation was included in (12)). It is likely that B also decreased, but B was assumed 1.0 in (12). Overestimation of B tends to give $u'/u'_\varepsilon < 1$ as observed (Figure 9*b*). *Nadaoka and Kondoh's* [1982] results (not shown) were biased very low (about 30% of u'_ε), consistent with their expectations that the high-pass-filter method used to separate turbulence from orbital velocities introduces relatively large errors.

5. CONCLUSIONS

Turbulence intensities in the natural surf zone were estimated using dissipation rates and a characteristic eddy length scale equal to 1/4 of the water depth. The dissipation rates were determined from wavenumber spectra found by applying Taylor's hypothesis to frequency spectra of 1/8-s hotfilm records. Turbulence intensities are largest near the surface and slowly decrease over the water column, consistent with strong mixing from the surface downward. The turbulence intensities agree very well with predictions from a macroscopic bore dissipation model which includes the effects of variations in wave frequency, broken-wave fraction, breaker coefficient, and wave-height to water-depth ratio. Good agreement was also found between previous laboratory turbulence observations and the macroscopic bore model. The large ratios of field-to-laboratory wave heights (e.g., 30:1) and frequencies (e.g., 10:1) indicate that bore-model scaling of surf zone turbulence intensity is robust over large differences in scale. Further experimental work is needed to extend and refine our preliminary findings. Data from above the trough level are needed, since turbulence levels may be maximum there. Robust, stable instruments which can distinguish all three components of the flow are still under development. Additional data sets are needed to determine the dependence of turbulence intensity on time since the passage of a bore and on breaker type.

APPENDIX A: BUBBLES

The signal from a constant-temperature hotfilm anemometer is corrupted by bubbles because air has much lower heat capacity than water. The hotfilm power (and therefore output voltage) required to maintain constant temperature is much smaller in air than in water at the same velocity [*Delhaye*, 1969]. The hotfilm output voltage signal during the passage of an air bubble is characterized by a steep-sided trough (Figure A1). *Resch et al.* [1974], studying turbulence levels in a hydraulic jump, used

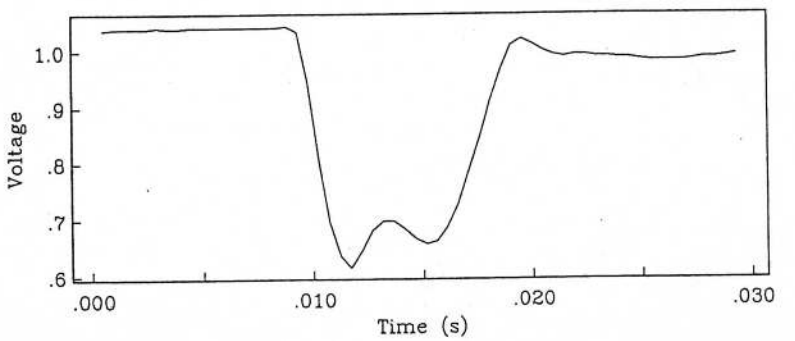

Fig. A1. Bubble signal in raw hotfilm voltage record.

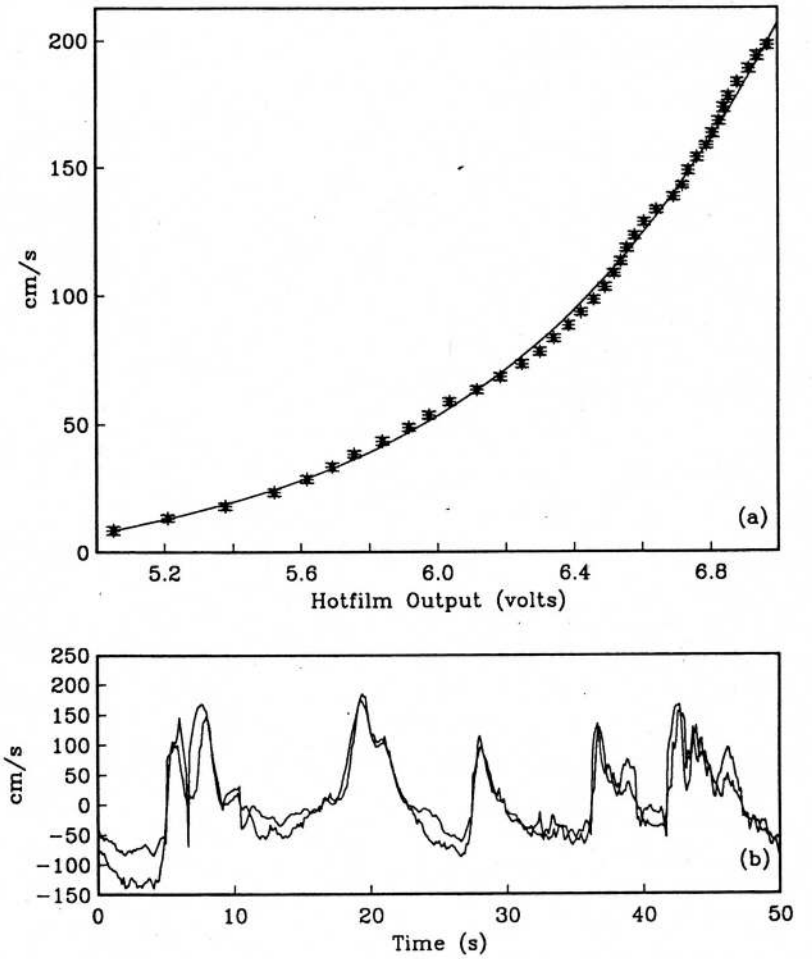

Fig. B1. (*a*) Typical hotfilm calibration curve. Error bars are ±1 standard deviation in each 5-cm/s bin. (*b*) Cross-shore velocity from the EM current meter and hotfilm (derectified to match the sign of the EM).

dropout voltage, the distance between the local signal maximum in the water and the minimum in the bubble, to recognize bubbles. However, there is no consistent dropout voltage in the surf zone due to widely varying bubble sizes and advective velocities, so we used a slope threshold method [*Wang*, 1985]. The maximum slope of the signal dropout is steeper than voltage changes associated with flow fluctuations. The hotfilms were sampled at 2048 Hz. Each bubble signal was replaced using linear interpolation, and the time series were then reduced by block averaging to 64 Hz.

APPENDIX B: CALIBRATION

The electromagnetic current meters (calibrated in a laboratory flow channel with an accuracy of a few cm/s; see *Guza et al.* [1988]) were used in situ to calibrate the hotfilms (which sense only the fluid speed). The absolute value of the EM current meter cross-shore velocity and the hotfilm voltage were reduced to 8 Hz. To reduce temporal lag problems caused by the small distance separating the hotfilm and EM current meter, the data points in each of the two time series were independently ranked by magnitude and then recoupled so that each hotfilm voltage was paired with the EM speed of the same rank. The data pairs were then averaged for bins spanning 5 cm/s. A log-log polynomial provided an acceptable and convenient fit to the resulting paired data. Each 512-s hotfilm time series was independently calibrated (Figure B1*a*). The EM and calibrated hotfilm time series were similar at sea-swell frequencies (Figure B1*b*).

Acknowledgments. This work was supported by the Office of Naval Research (Coastal Sciences) under grant N00014-89-J-1059; by NOAA, National Sea Grant Program, Department of Commerce, under grant NA85AA-D-SG140, project R10E-3, and grant NA89AA-D-SG138, project R/CZ-90, through the California Sea Grant College Program; and by the California State Resources Agency. R.E.F. gratefully acknowledges support from the California Department of Boating and Waterways. Thanks to Bill Boyd and Mike Clifton for assistance with the field work, to Marcel Stive for generously sharing his laboratory data, and to Carl Gibson, Kazuo Nadaoka, Chuck Van Atta, and Clinton Winant for helpful discussions.

REFERENCES

Baker, M. A., and C. H. Gibson, Sampling turbulence in the stratified ocean: Statistical consequences of strong intermittency, *J. Phys. Oceanogr.*, *17*, 1817-1836, 1987.

Battjes, J. A., Modelling of turbulence in the surf zone, in *Proceedings, Symposium on Modelling Techniques*, pp. 1050-1061, San Francisco, Calif., Am. Soc. Civ. Eng., N.Y., 1975.

Battjes, J. A., Surf zone dynamics, *Annu. Rev. Fluid Mech.*, *20*, 257-293, 1988.

Bradshaw, P., *An Introduction to Turbulence and Its Measurement*, 218 pp., Pergamon, New York, 1971.

Crawford, W. R., and T. R. Osborne, Microstructure measurements in the Atlantic equatorial undercurrent during GATE, *Deep Sea Res.*, *26*, GATE suppl. II, 285-308, 1980.

Delhaye, J. M., Hot-film anemometry in two-phase flow, in *Proceedings, 11th National ASME/AIChE Heat Transfer Conference*, pp. 58-68, American Society of Chemical Engineers/American Institute of Chemical Engineers, New York, 1969.

Flick, R. E., R. T. Guza, and D. L. Inman, Elevation and velocity measurements of laboratory shoaling waves, *J. Geophys. Res.*, *86*, 4149-4160, 1981.

Fuhrboter, A., Air entrainment and energy dissipation in breakers, *Proc. 12th Coastal Eng. Conf.*, *1*, 391-398, Am. Soc. Civ. Eng., N.Y., 1970.

Gibson, C. H., Laboratory, numerical, and oceanic fossil turbulence inrotary and stratified flows, *J. Geophys. Res.*, *96*(C7), 12,549-12,566, 1991.

Grant, H. L., R. W. Stewart, and A. Moilliet, Turbulence spectra from a tidal channel, *J. Fluid. Mech.*, *12*, 241-268, 1962.

Guza, R. T., M. C. Clifton, and F. Rezvani, Field intercomparisons of electromagnetic current meters, *J. Geophys. Res.*, *93*(C8), 9302-9314, 1988.

Hattori, M., and T. Aono, Experimental study on turbulence structures under spilling breakers, in *The Ocean Surface*, edited by Y. Toba and H. Mitsuyasa, pp. 419-424, D. Reidel, Norwell, Mass., 1985.

Hinze, J. O., *Turbulence*, 790 pp., McGraw-Hill, New York, 1975.

Kitaigorodskii, S. A., M. A. Donelan, J. L. Lumley, and E. A. Terray, Wave-turbulence interactions in the upper ocean, Part II, Statistical characteristics of wave and turbulent components of the random velocity field in the marine surface layer, *J. Phys. Oceanogr.*, *13*, 1988-1999, 1983.

Kolmogorov, A. N., A refinement of previous hypothesis concerning the local structure of turbulence in a viscous fluid for very large Reynolds number, *J. Fluid Mech.*, *13*, 82-85, 1962.

Lin, C. C., On Taylor's hypothesis and the acceleration terms in the Navier-Stokes equations, *Q. Appl. Math.*, *10*, 295, 1953.

Lumley, J. L., and E. A. Terray, Frequency spectra of frozen turbulence in a random wave field, *J. Phys. Oceanogr.*, *13*, 2000-2007, 1983.

Nadaoka, K., and T. Kondoh, Laboratory measurements of velocity field structure in the surf zone by LDV, *Coastal Eng. Jpn.*, *25*, 125-145, 1982.

Nadaoka, K., M. Hino, and Y. Koyano, Structure of the turbulent flow field under breaking waves in the surf zone, *J. Fluid Mech.*, *204*, 359-387, 1989.

Oboukhov, A. M., Some specific features of atmospheric turbulence, *J.Fluid Mech.*, *13*, 77-81, 1962.

Resch, F. J., and H. J. Leutheusser, Mesures des tensions de Reynolds dans le ressaut hydraulique, *J. Hydraul. Res.*, *10*, 409-429, 1972.

Resch, F. J., H. J. Leutheusser, and S. Alemu, Bubbly two-phase flow in hydraulic jump, *J. Hydraul. Div., Am. Soc. Civ. Eng*, *100*, 137-149, 1974.

Skjelbreia, J. E., Observations of breaking waves on sloping bottoms by use of laser Doppler velocimetry, Ph.D. thesis, 176 pp., Calif. Inst. of Technol., Pasadena, May 1987.

Stive, M. J. F., Velocity and pressure field of spilling breakers, *Proc. 17th Int. Conf. Coastal Eng.*, *1*, 547-566, Am. Soc. Civ. Eng., 1980.

Svendsen, I. A., Analysis of surf zone turbulence, *J. Geophys. Res.*, *92*, 5115-5124, 1987.

Tennekes, H., and J. L. Lumley, *A First Course in Turbulence*, 300 pp., MIT Press, Cambridge, Mass., 1972.

Thornton, E. B., Energetics of breaking waves within the surf zone, *J. Geophys. Res.*, *84*, 4931-4938, 1979.

Thornton, E. B., and R. T. Guza, Transformation of wave height distribution, *J. Geophys. Res.*, *88*(C10), 5925-5938, 1983.

Wang, S. L., Three-dimensional turbulence structure measurements in air/water two-phase flow, Ph.D. thesis, 442 pp., Rensselaer Polytechnic, Troy, N.Y., Aug. 1985.

R. E. Flick, California Department of Boating and Waterways, 9500 Gilman Drive, LaJolla, CA 92093-0209.

R. George and R. T. Guza, Center for Coastal Studies, Scripps Institution of Oceanography, 9500 Gilman Drive, La Jolla, CA 92093-0209.

(Received February 25, 1993;
revised August 3, 1993;
accepted September 8, 1993.)